Article

Current Biology

A miniaturized nigrostriatal-like circuit regulating locomotor performance in a protochordate

Graphical abstract

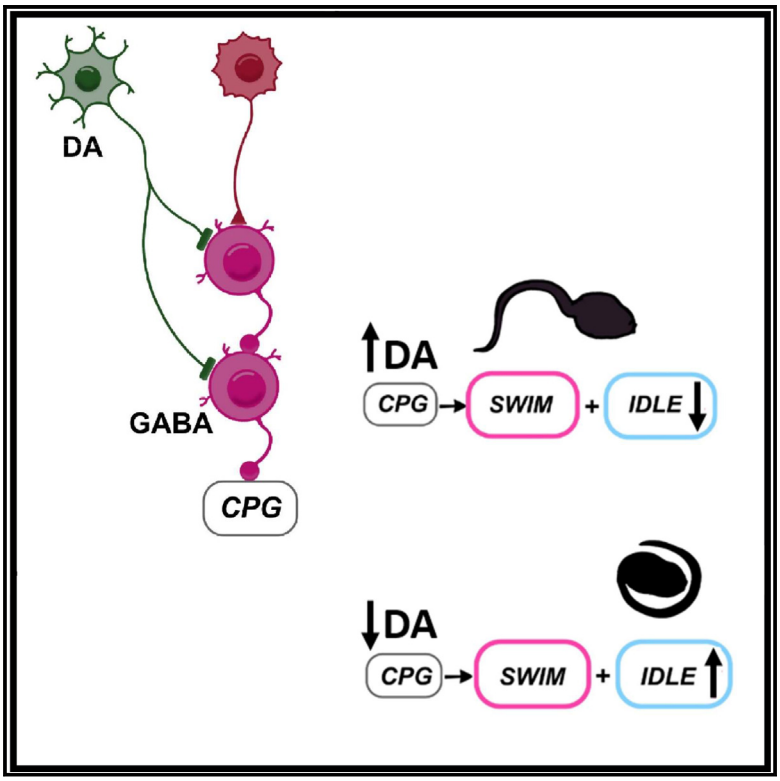

Highlights

- *Oikopleura*'s miniaturized brain contains only 2 dopaminergic neurons
- Dopamine receptor expression reveals GABAergic neurons as principal synaptic targets
- GABAergic neurons comprise a disinhibitory projection to the locomotor CPG
- Dopamine regulates locomotor efficiency by adjusting the idling/swimming ratio

Authors

Oleg Tolstenkov, Yana Mikhaleva, Joel C. Glover

Correspondence

joel.glover@medisin.uio.no

In brief

Tolstenkov et al. show that locomotion in a urochordate is regulated by a highly miniaturized, dopamine-modulated disinhibitory circuit, similar and likely homologous to the vertebrate nigrostriatopallidal system. This form of motor control thus predates vertebrates and has been maintained in the face of extreme evolutionary CNS miniaturization.

Tolstenkov et al., 2023, Current Biology *33*, 3872–3883
September 25, 2023
https://doi.org/10.1016/j.cub.2023.08.015

CellPress

CellPress
OPEN ACCESS

Current Biology

Article

A miniaturized nigrostriatal-like circuit regulating locomotor performance in a protochordate

Oleg Tolstenkov,[1,3] Yana Mikhaleva,[1,3] and Joel C. Glover[1,2,4,*]
[1]Sars International Centre for Marine Molecular Biology, University of Bergen; Thormøhlensgate 55, 5008 Bergen, Norway
[2]Laboratory of Neural Development and Optical Recording (NDEVOR), Department of Molecular Medicine, Institute of Basic Medical Sciences, University of Oslo, Sognsvannsveien 9, 0372 Oslo, Norway
[3]These authors contributed equally
[4]Lead contact
*Correspondence: joel.glover@medisin.uio.no
https://doi.org/10.1016/j.cub.2023.08.015

SUMMARY

To gain insight into the evolution of motor control systems at the origin of vertebrates, we have investigated higher-order motor circuitry in the protochordate *Oikopleura dioica*. We have identified a highly miniaturized circuit in *Oikopleura* with a projection from a single pair of dopaminergic neurons to a small set of synaptically coupled GABAergic neurons, which in turn exert a disinhibitory descending projection onto the locomotor central pattern generator. The circuit is reminiscent of the nigrostriatopallidal system in the vertebrate basal ganglia, in which disinhibitory circuits release specific movements under the modulatory control of dopamine. We demonstrate further that dopamine is required to optimize locomotor performance in *Oikopleura*, mirroring its role in vertebrates. A dopamine-regulated disinhibitory locomotor control circuit reminiscent of the vertebrate nigrostriatopallidal system was thus already present at the origin of ancestral chordates and has been maintained in the face of extreme nervous system miniaturization in the urochordate lineage.

INTRODUCTION

The evolution of motor control systems at the invertebrate-to-vertebrate transition is poorly understood.[1–3] Understanding motor circuits in protochordates, which split from vertebrates at the base of the chordate lineage 600 million years ago,[4] can provide insight into the origin of key elements of vertebrate motor control. Of particular interest are the urochordates, or tunicates, the closest living relatives to vertebrates[5] and thus likely to exhibit the greatest degree of invertebrate-vertebrate brain homology. Urochordates have been subject to evolutionary miniaturization of both the genome and the brain,[6,7] and with fewer than 200 neurons total, they may be expected to harbor the most crucial elements of motor circuitry shared with vertebrates. However, higher-order motor regulatory circuitry is poorly characterized in protochordates.

In vertebrates, dopamine plays a critical role in regulating motor control networks in the basal ganglia. Dopaminergic neurons in the substantia nigra pars compacta (SNpc) project to inhibitory GABAergic medium spiny neurons (MSNs) in the striatum, which in turn project to inhibitory GABAergic neurons in the pallidum, whose output regulates the release of specific movements. Activation of D1 and D2 dopamine receptors leads to reciprocal excitability changes in the MSNs giving rise to direct and indirect striatopallidal-output pathways, respectively, thus promoting the release of specific movements through disinhibition.[8] Adrenergic receptors (ADRs) on MSNs are also involved, but their role is less well understood in an overall functional context, although they are believed to interact synergistically with dopamine receptors.[9,10]

The pivotal function of dopamine in regulating movement comes into sharp relief in the clinical context of Parkinson's disease, in which depletion of dopamine in the striatum caused by degeneration of dopaminergic neurons in the SNpc leads to a severely hypokinetic state.[11–13] By contrast, hyperkinesia and hyperactivity can result from elevated levels of dopamine in the striatum, such as caused by specific medication regimes or drug use (L-3,4-dihydroxyphenylalanine [L-DOPA] induced hyperkinesia, amphetamine-induced locomotor stimulation).[14]

The role of dopamine in regulating the direct and indirect striatopallidal-output pathways has been described in several craniate taxa, including mammals, birds, reptiles, amphibians, and lampreys (reviewed in Wullimann[15] and Grillner[16]). Homology to a similarly organized system in insects has been proposed,[17] and an influence of dopamine on movement has been documented in numerous invertebrates, including the protochordate *Ciona*.[18,19] However, it is not clear whether a form of the nigrostriatopallidal projection exists in protochordates, located at the base of the chordate evolutionary tree and with a central nervous system (CNS) homologous to that of vertebrates. This is of particular interest with respect to urochordates, some species of which exhibit features of behavioral choice in the initiation and selection of movement patterns despite having a severely miniaturized CNS.[4,20]

Here, we utilize molecular approaches to identify dopaminergic and GABAergic neurons and their synaptic targets in the appendicularian urochordate *Oikopleura dioica*, whose CNS follows the

vertebrate developmental bauplan but contains only about 130 neurons.[4] We further assess the effect of dopamine supplementation and depletion on spontaneous locomotor behavior. We find that (1) dopaminergic output selectively targets GABAergic neurons rather than glutamatergic or cholinergic neurons, (2) GABAergic neurons are synaptically coupled and provide a descending inhibitory input to the locomotor central pattern generator (CPG) that can be disinhibited in the intact animal, and (3) locomotor regulation by dopamine parallels that seen in vertebrates: augmented levels promote and diminished levels impede forward propulsive locomotion. These features align with the general functional organization of the vertebrate nigrostriatopallidal system, indicating that a basal ganglia-like function was established at the base of the chordate tree and has been maintained in *Oikopleura* in a minimal circuit sufficient to regulate movement states despite involving only a handful of neurons.

Background on *Oikopleura*'s lifestyle

A short introduction to its unusual lifestyle will assist readers unfamiliar with *Oikopleura*. *Oikopleura* develops rapidly, achieving a motile larval stage within a few hours post fertilization (hpf) and a behaviorally mature form with a complete complement of neurons and a well-developed repertoire of distinct behaviors[4,20] in less than a day. In contrast to ascidian tunicates like *Ciona*, which metamorphose into sessile adults, *Oikopleura* remains free-swimming throughout its short, 1-week lifespan (Figure S1).[21] Its protein- and cellulose-containing tunic is excreted by the epithelium of the head and then expands into a structure called the "house" that dwarfs the animal itself. While residing within the house, *Oikopleura* engages in undulatory movements of the tail that drive water through funnels and filters in the house that facilitate the capture of algae for food. *Oikopleura* leaves the house if stressed or if the filters become clogged, and then creates a new house. While outside of its house, *Oikopleura* exhibits undulatory swimming movements distinct from the in-house filtering movements and also bending movements in response to sensory stimulation or as a warm-up to the initiation of swimming.[20] The CNS of *Oikopleura* is believed to have undergone extensive evolutionary miniaturization since it has substantially fewer neurons than the more basal protochordate amphioxus (for more details, see Glover[4] and Kreneisz and Glover[20]).

RESULTS

Oikopleura has only two putative dopaminergic neurons and expresses a functional dopamine receptor

A search of the *Oikopleura dioica* genome identified genes predicted to encode tyrosine hydroxylase (TH), DOPA decarboxylase (AADC), and dopamine β-hydroxylase (DBH), which respectively catalyze the conversion of tyrosine to L-DOPA, of L-DOPA to dopamine, and of dopamine to noradrenaline. Multiple sequence alignment of the Od-TH gene (GenBank: CBY12061.1) to the TH genes of *Danio rerio* (GenBank: XP_005164791.1), *Homo sapiens* (GenBank: AAI04968.1), *Ciona intestinalis* (GenBank: NP_001027967.1), *Drosophila melanogaster* (GenBank: NP_476897.1), and *Rattus norvegicus* (GenBank: NP_036872.1) showed amino acid sequence conservation in the catalytic domain of the predicted Od-TH protein (48% identity, 65% positives to vertebrate TH), including residues forming the binding pocket for iron ion (H310-H315-E355) and S374, an important catalytic site.[22–24] 3D protein structure prediction by the Phyre2 online service[25] confirmed the presence of catalytic and regulatory domains in the Od-TH sequence (not shown).

Od-TH gene transcripts were expressed in only two neurons situated in the middle of the cerebral ganglion, considered homologous to the vertebrate forebrain and midbrain.[26,27] Transcripts could be detected reliably in all animals by 5 hpf and remained specific to the two neurons during all developmental stages through metamorphosis (Figures 1A–1E).

Od-AADC gene (GenBank: CBY20168.1, GSOIDG00000153001) transcripts colocalized with Od-TH transcripts (Figure S2A), indicating the potential for dopamine synthesis in these neurons. However, Od-DBH (GenBank: CBY11687.1) gene transcripts were not expressed in the CNS but rather in some peripheral sensory cells (Figure S2B), suggesting that the two TH/AADC+ neurons can synthesize dopamine but not noradrenaline.

We then searched for potential dopamine receptor genes. As is the case for the sessile ascidian urochordate *Ciona*, the *Oikopleura dioica* genome contains no sequence with substantial resemblance to the bilaterian dopamine receptor genes.[26,28,29] We therefore performed a protein blast of the *Ciona intestinalis* gene proposed to encode an α2-ADR (GenBank: XP_002120235.3)[26] and obtained two *Oikopleura* protein sequence hits (GenBank: CBY09491.1 and GenBank: CBY37057.1) (Figure S3). These are two splice variants of the same gene (GSOIDG00008492001), differing in their N-terminal and C-terminal domains but sharing the same core sequence of the transmembrane domain and intracellular loop 3, which are usually responsible for G-protein coupling. To assess the relationship of this protein to ADRs and dopamine receptors identified in vertebrates, we obtained a maximum likelihood tree, including *Ciona* and vertebrate ADR proteins and the vertebrate dopamine D2 receptor (DRD2) protein and found a closer phylogenetic relationship to DRD2 than to ADR (Figure S4). We refer to this *Oikopleura* protein as the *Oikopleura* dopamine-adrenaline receptor (Od-DAR) due to its dual neurotransmitter binding (see below).

Standard qPCR of Od-TH and Od-DAR gene transcripts from 1 to 12 hpf revealed a major peak for each, with the Od-TH peak preceding the Od-DAR peak (Figure 1Ai). *In situ* hybridization for Od-DAR, using a probe selective for a sequence common to the long and short variants, showed a broad pattern of expression in different tissues, including neurons in the cerebral ganglion, caudal ganglion, and caudal nerve cord, as well as in the buccal glands, spiracles, and gut (Figures 1A′–1E′).

To determine whether the Od-DAR protein binds dopamine and triggers G-protein-mediated signaling, we performed experiments using HEK293 cells heterologously co-expressing the Od-DAR protein and a mouse G-protein. Exposure to 50 μM dopamine or noradrenaline triggered release of Ca^{2+} from intracellular stores (Figure S5; Video S1), indicating that Od-DAR binds both neurotransmitters and mediates downstream G-protein interaction. The response was similar to the response to activating a mouse ADR in the same heterologous cell expression system (not shown).

Putative GABAergic neurons identified as principal postsynaptic targets

We next identified potential postsynaptic targets of the putative dopaminergic neurons through double fluorescence *in situ*

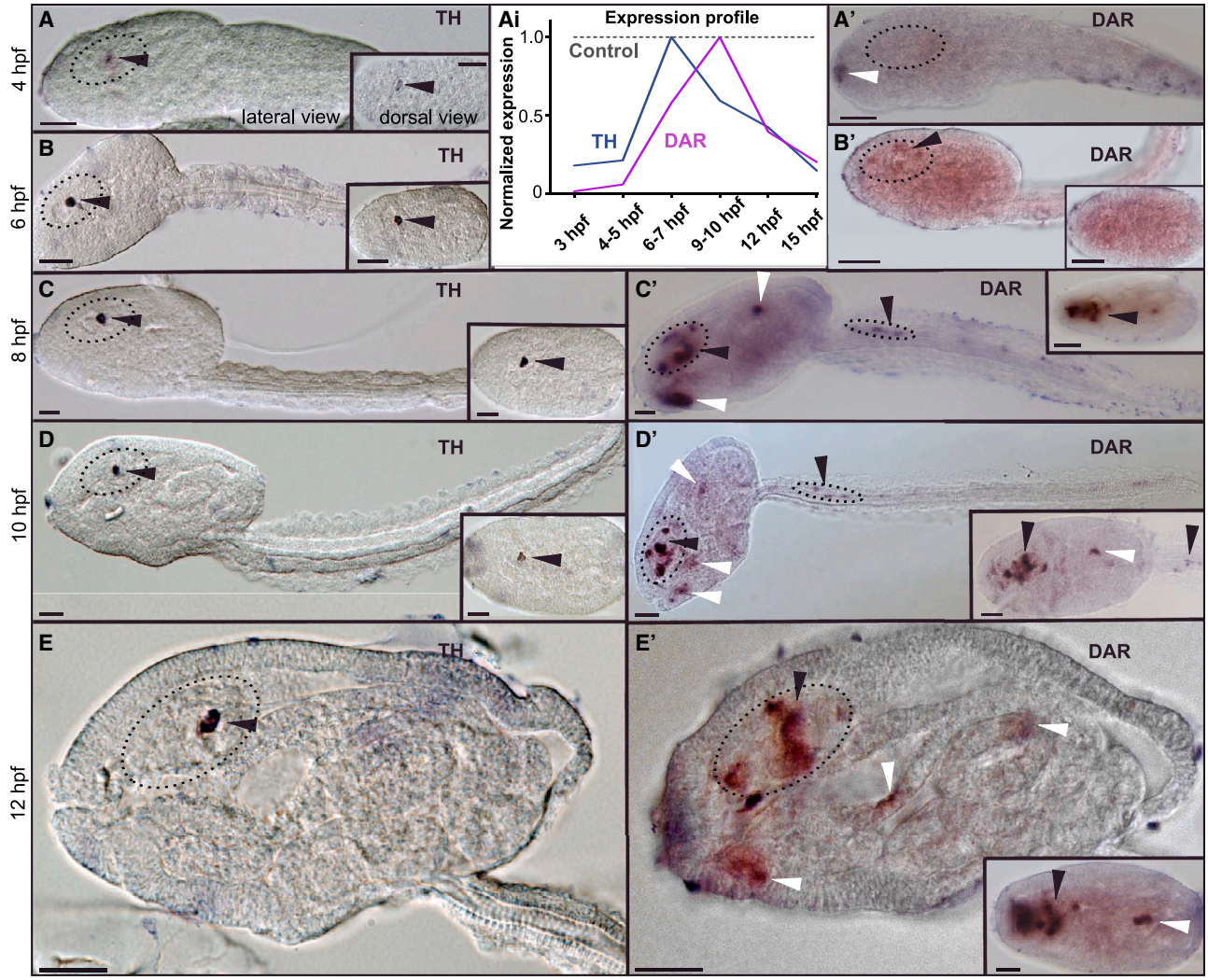

Figure 1. Expression of Od-TH and Od-DAR transcripts during *Oikopleura* development

(A–E) *In situ* hybridization of (A–E) *Oikopleura dioica* tyrosine hydroxylase (TH) and (A′–E′) dopamine-adrenergic receptor (DAR) transcripts at 4–12 hpf in lateral and dorsal (insets) views. The cerebral ganglion is circumscribed by a dotted line in all lateral view panels, as is the caudal ganglion in (C′) and (D′). Black arrows indicate expression within the ganglia, and white arrows in peripheral structures.

(Ai) Temporal profile of Od-TH and Od-DAR expression normalized to expression of the housekeeping gene RPL23 (qPCR on 3 pooled batches of embryos at each of the indicated stages). Scale bars, 10 μm.

See also Figures S2–S5, Table S1, and Video S1.

hybridization and colocalization analysis of Od-DAR versus either Od-TH (putative dopaminergic neurons), Od-GAD (glutamic acid decarboxylase, indicating putative GABAergic neurons), Od-ChAT (choline acetyltransferase, indicating motoneurons), or Od-VGluT (vesicular glutamate transporter, indicating putative glutamatergic neurons) (Figure 2). We found that Od-DAR co-expressed with Od-TH during a brief developmental period (9–11 hpf), suggesting a transient autoreceptor role. Otherwise, we found consistent and unequivocal Od-DAR co-expression in all Od-GAD-expressing neurons in the cerebral and caudal ganglia (8 in the cerebral ganglion, 3 in the caudal ganglion; Figures 2BI and 2CI), but not in Od-VGluT- or Od-ChAT-expressing neurons (Figures 2BII, 2CII, and 2CIII). Another 5 Od-DAR-expressing neurons in the rostral region of the cerebral ganglion were neither Od-GAD+, Od-VGluT+, nor Od-ChAT+ (Figure 2BI). Thus, putative GABAergic neurons represent principal synaptic targets of the putative dopaminergic neurons, and all of them receive dopaminergic innervation, based on the expression of the functional dopamine receptor Od-DAR.

Putative GABAergic neurons engage in a disinhibitory projection to the locomotor CPG

In a separate study to be published elsewhere, we have characterized *Oikopleura* GABA receptors molecularly and genomically (Od-GABA-Rs; Y.M., unpublished data). Here, we again used double *in situ* hybridization and colocalization analysis and found that all 11 Od-GAD-expressing (putative GABAergic) neurons (8 in the cerebral ganglion and 3 in the caudal ganglion) express Od-GABA-R transcripts, consistent with the presence of

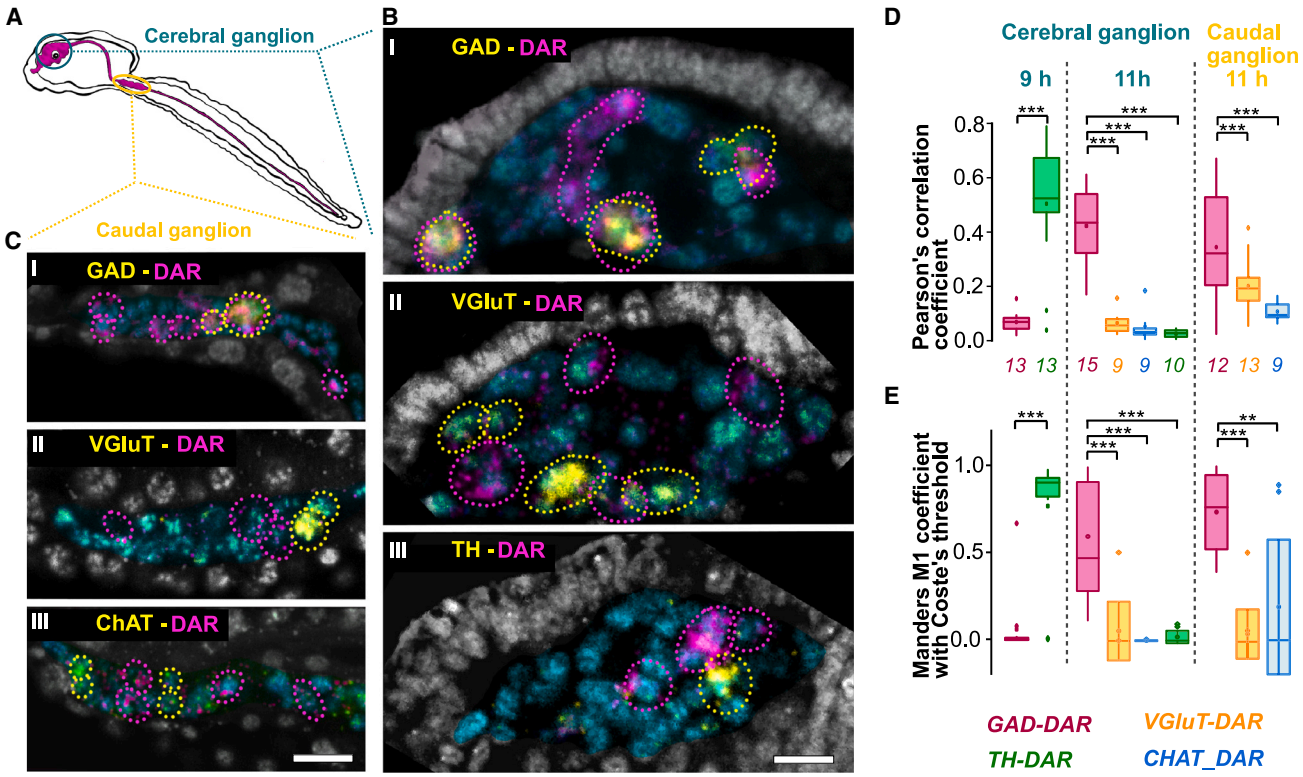

Figure 2. Colocalization analysis of Od-DAR and neurotransmitter-specific gene transcripts

(A) Drawing of side view of *Oikopleura* with cerebral and caudal ganglia circumscribed in green and yellow, respectively.

(B and C) Fluorescence *in situ* hybridization in the cerebral (B) and caudal (C) ganglia at 11 hpf of *Oikopleura* dopamine-adrenergic receptor (Od-DAR, magenta) versus glutamate decarboxylase (Od-GAD, yellow) (BI and CI), vesicular glutamate transporter (Od-VGluT) (BII and CII), tyrosine hydroxylase (Od-TH) (BIII) or choline acetyltransferase (Od-ChAT) (CIII). Individual neurons or small clusters of neurons expressing the indicated transcript are circumscribed by color-coded dotted lines. Nuclear staining of neurons in light blue and of non-neural cells in gray. Note that at this stage, colocalization of Od-TH and Od-DAR is no longer evident (BIII).

(D and E) Quantification of colocalization between Od-DAR and neurotransmitter-specific gene transcripts using Pearson's (D) and Manders M (E) correlation coefficients. *$p < 0.05$; **$p < 0.01$; ***$p < 0.001$. Sample sizes (shown in D for both D and E) indicate numbers of embryos from two batches. Statistical tests in (D) and (E): Mann-Whitney U-test and Kruskal-Wallis ANOVA followed by post hoc Dunn's test. Note that there are outliers for VGluT-DAR and ChAT-DAR colocalization, particularly in the caudal ganglion, but no consistent colocalization as is the case for GAD-DAR. Scale bars, 5 μm. Box and whisker plots show mean (small square within box), median (horizontal line within box), lower and upper quartiles (lower and upper box limits), maximum and minimum (upper and lower limits of whiskers), and outliers (points above or below whiskers).

See also Figures S2 and S6 and Table S1.

reciprocal inhibitory connections and/or disinhibitory projections (Figure S6). This accords with interconnections between putative GABAergic neurons documented in the connectome of the ascidian urochordate *Ciona*.[30,31]

The presence of a disinhibitory GABAergic projection onto the locomotor CPG in *Oikopleura* is supported by two previously published findings. Bollner et al. demonstrated the presence of GABA-immunoreactive axons in the nerve that connects the cerebral ganglion to the caudal ganglion.[32] Kreneisz and Glover demonstrated that the cerebral ganglion exerts a descending inhibitory influence on the locomotor CPG in the caudal ganglion, which can be disinhibited.[20] They found that severing the connecting nerve, by separating the tail from the rest of the animal, led to swimming or bending behavior that continued indefinitely (up to several hours, in contrast to the few seconds' duration of swimming or bending episodes exhibited by intact animals). Thus, there must be a source of tonic inhibition from the cerebral to the caudal ganglion that normally prevents swimming or bending and that is transiently inactivated when swimming or bending is expressed.

To provide more direct evidence that the descending inhibition to the locomotor CPG is GABAergic, we isolated tails to release continuous swimming or bending movements and then applied GABA or glycine to the isolated tails and to intact animals for comparison. Application of GABA (50 μM) to continuously moving tails abruptly inhibited the movement in a large majority of cases, whereas application of glycine did not (Figure S6; Video S2). Application of 50 μM GABA to intact animals did not stop spontaneous episodic movements but rather increased the number of turns within a trajectory and thereby constrained the overall trajectory (not shown).

Spontaneous open-field locomotion of *Oikopleura* comprises episodes of swimming, idling, and quiescence

To assess the influence of dopamine on locomotor behavior, we placed mature (24 hpf) *Oikopleura* that had left the house in an open-field and filmed spontaneous movements. Movement trajectories analyzed at low magnification (see STAR Methods)

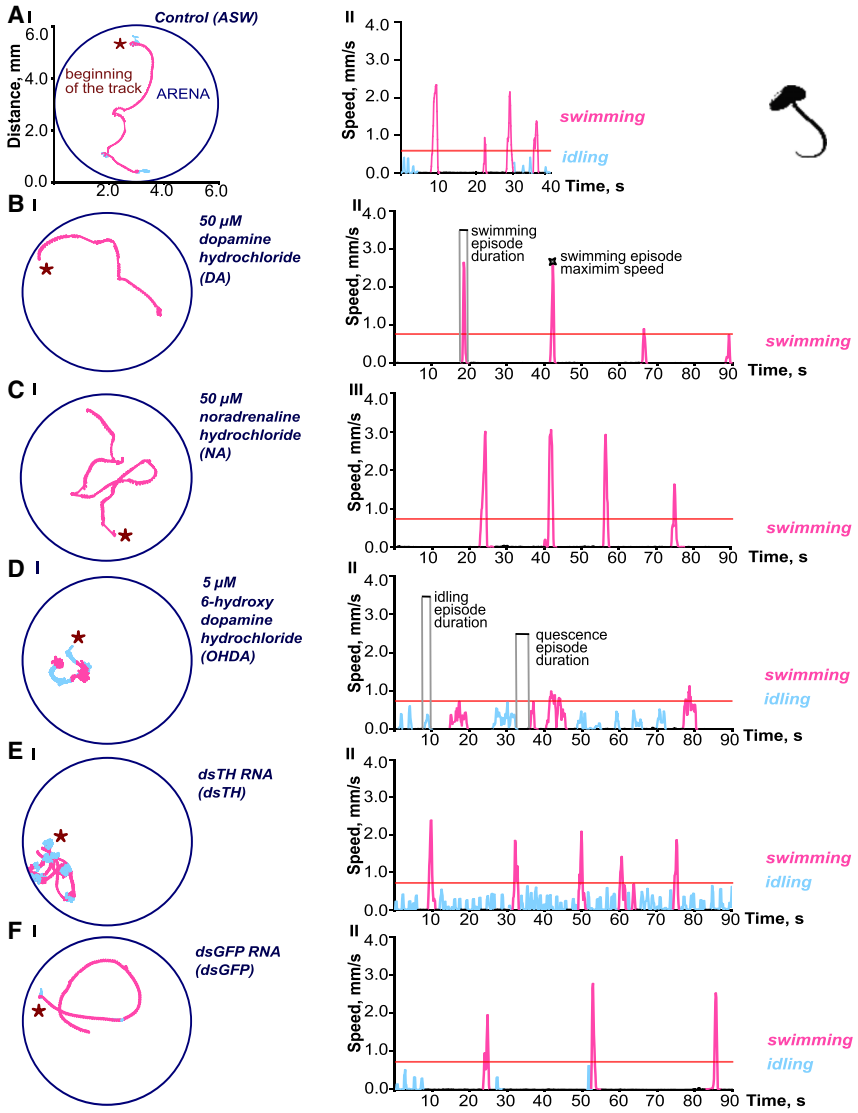

Figure 3. Representative movement trajectories and corresponding forward propulsion versus time graphs of D1 *Oikopleura* under different experimental conditions

(A) (I) representative trajectory and (II) forward propulsion graph of a control animal in ASW.

(B–F) Representative trajectories (I) and forward propulsion graphs (II) of individual animals incubated in 50 μM dopamine (B), 50 μM noradrenaline (C), or pre-treated with 5 μM 6-hydroxydopamine (D) or injection of TH dsRNA (E) or GFP dsRNA (negative dsRNA control) (F). Swimming and idling are color-coded (pink and blue, respectively, with the threshold between the two at 0.7 mm/s [shown by the horizontal pink line in the forward propulsion graphs]), and episodes of quiescence are indicated by the baseline between movement episodes.

See also Figure S7 and Videos S3, S4, S5, and S6.

comprised episodes of forward propulsive swimming (speeds ≥ 0.7 mm/s) interspersed with episodes of "idling" (forward propulsion ≥ 0.09 mm/s but < 0.7 mm/s) and episodes of quiescence (movement < 0.09 mm/s) (Figure 3A; Video S3). The rationale for these speed thresholds is described in STAR Methods but, in short, is based on the fact that swimming generates forward propulsion of at least one body length per second, and drifting in the absence of any tail movement can be as high as 0.09 mm/s. We note that in some instances (including some presented in the supplemental video material) animals collided with the wall of the arena during a recording session, an event that could affect behavior through mechanosensory stimulation or simply impede movement. However, the behavioral differences we document below were apparent even when such events were not included in the analysis.

Higher magnification analysis of idling showed that it comprised a series of bending movements that sent the animal into a slow gyratory motion with a circular trajectory with no net forward vector (Figures 4A and 4B). Consistent with this, power spectral density analysis revealed a maximum frequency of around 40 Hz during swimming episodes (Figures 4C and 4D), corresponding to the frequency of swimming previously characterized,[20] but no well-defined frequency maximum during idling episodes (Figures 4C–4E). The overall animal displacement occurring during swimming episodes was distinctly greater than that occurring during idling episodes (Figure 4F).

Dopamine increases overall locomotor efficiency

To investigate whether the dopaminergic system regulates *Oikopleura*'s locomotor state, we assessed spontaneous locomotion during pharmacological and transcriptional interventions targeting the putative dopaminergic neurons and their synapses (Figures 3 and 5). Pharmacological manipulations required relatively high concentrations of compounds to overcome the diffusion barrier presented by the outer epithelium and integument.

Exposure to exogenous dopamine (50 μM) produced a distinct behavioral phenotype. The incidence and duration of swimming episodes did not change (Figures 3A, 5A, and 5BI), but idling episodes occurred substantially less frequently and in some animals were eliminated, such that animals either swam or were quiescent (Figures 3B, 5AII, and 5BII; Video S4). Quantitatively, the average total time spent idling decreased to about 40% of the control level. By contrast, the duration of quiescent episodes increased significantly from 3.03 ± 1.8 s in untreated control animals to 7.98 ± 5.76 s in animals exposed to dopamine (Figure 3B). Average forward velocity during swimming episodes was elevated (2.12 ± 0.42 mm/s compared with 1.65 ± 0.35 mm/s in controls), indicating a higher swimming cycle frequency, as swimming velocity is directly proportional to cycle frequency (Figure 4E). Together, these effects led to a significant increase in the overall mean speed of forward propulsion during

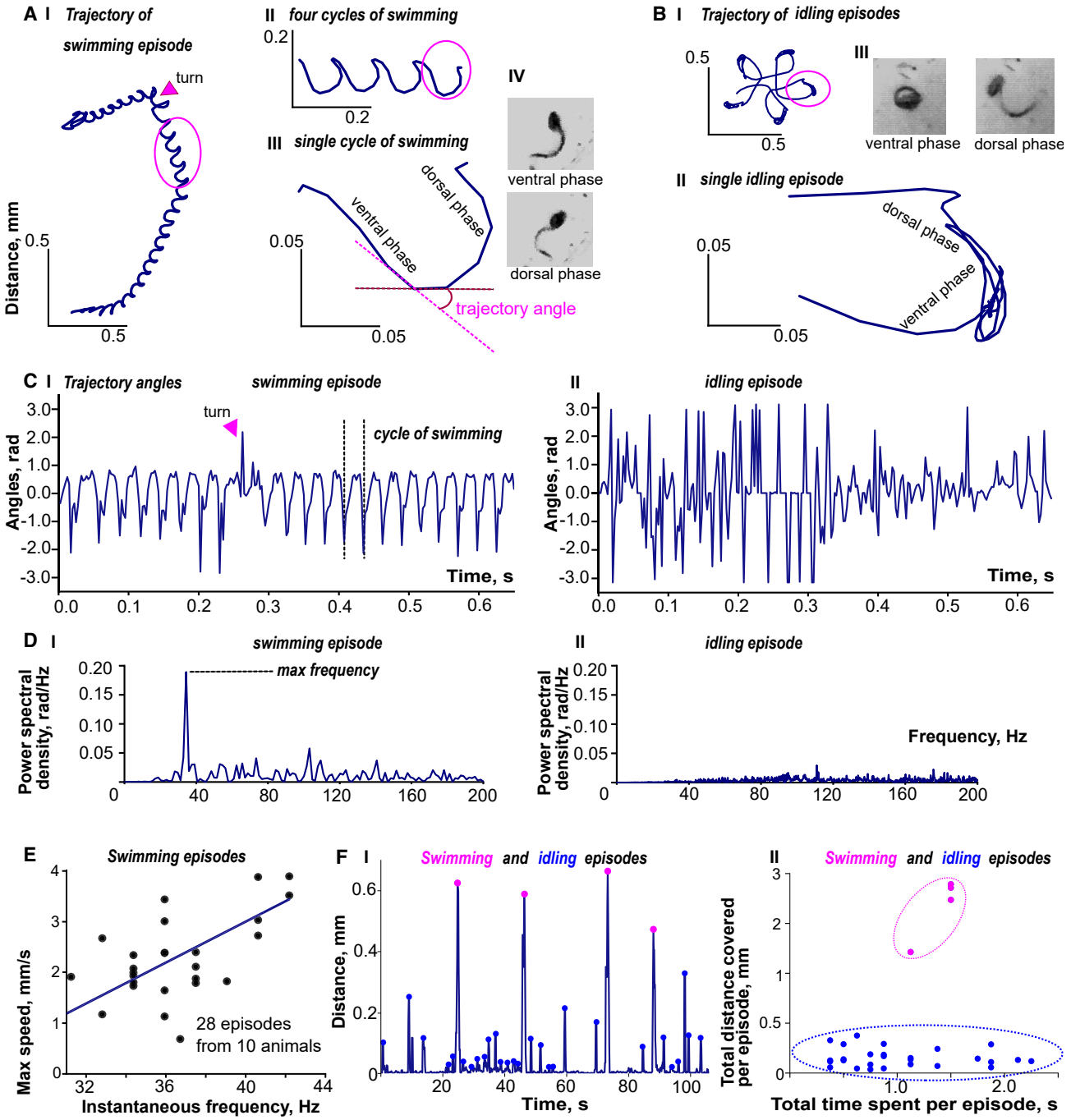

Figure 4. Movement trajectories of D1 *Oikopleura* outside of the house

(A) (I) Trajectory of representative swimming episode (arrowhead indicates a turn in swimming direction). (II) Trajectory detail during four consecutive cycles of swimming. (III) Single cycle of swimming with indicated trajectory angle at the transition from ventral phase to dorsal phase of tail movement, with corresponding body postures show in (IV).

(B) (I) Trajectory of representative idling episode. (II) Trajectory detail during single loop of an idling episode, with the corresponding body postures shown in (III).

(C) Trajectory angles in radians versus time during a swimming episode (I, arrowhead indicates the turn in swimming direction) with a single cycle of swimming indicated, and during an idling episode (II).

(D) Power spectra of trajectory angle frequencies for representative swimming (I) and idling (II) episodes. Maximum frequency in the swimming episode is indicated.

(E) Relation of swimming cycle instantaneous frequency to maximum speed of forward propulsion, in 10 animals obtained from two batches.

(F) (I) Distance plotted versus time for a representative animal in control condition with swimming and idling episodes indicated respectively by magenta and blue dots at the distance maxima. (II) Dispersal (total distance covered per episode) during the swimming and idling episodes for the same animal. Note the distinct gap in the distribution, indicating that 0.7 mm/s can be used as a velocity threshold for distinguishing swimming and idling.

See also Videos S3, S4, S5, and S6.

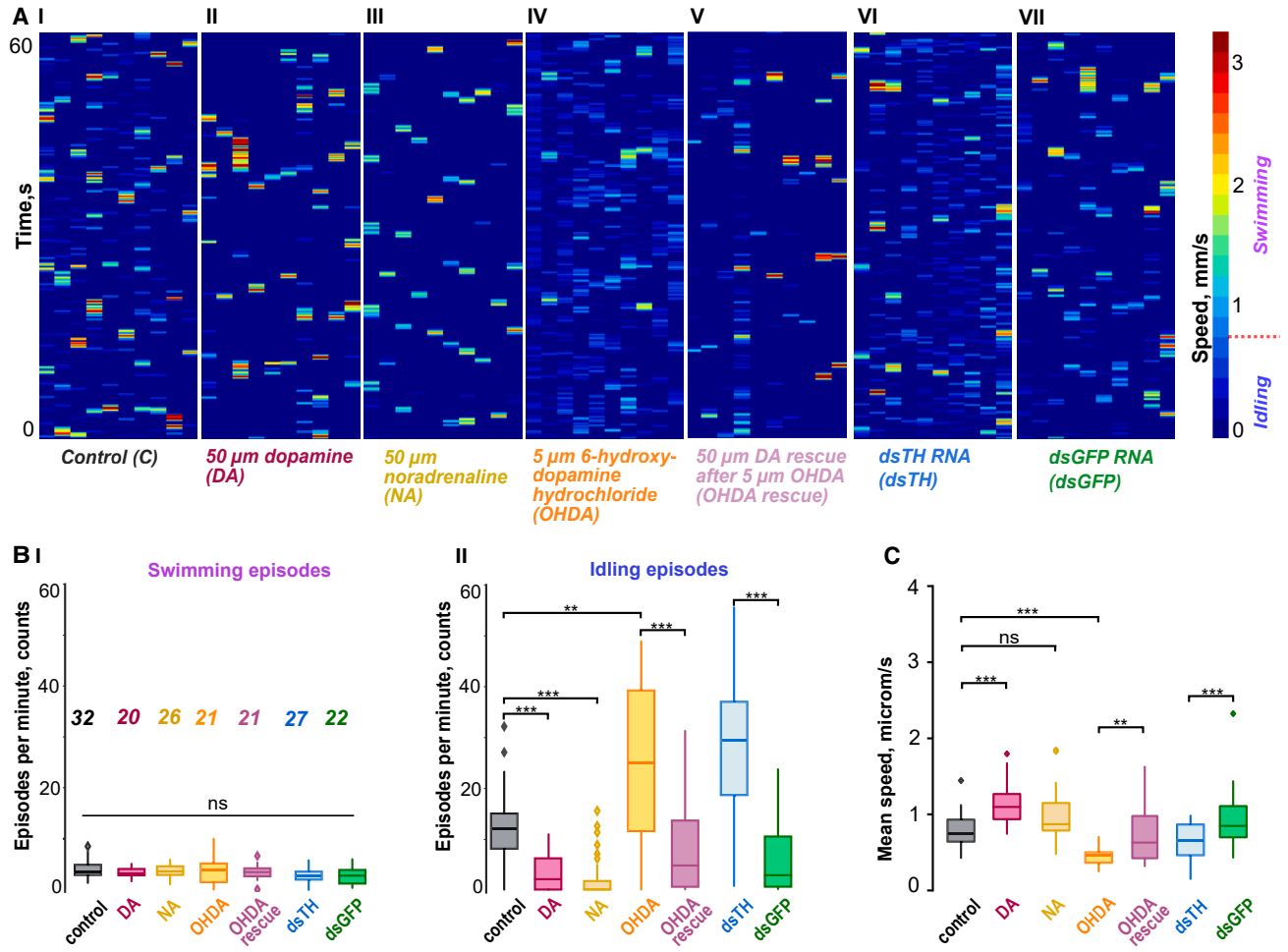

Figure 5. Quantitative assessment of different experimental manipulations of dopaminergic transmission on locomotor behavior

(A) Heat maps of 10 animals per experimental condition (each column represents one animal) during 1-min recording (starting at 0 s at the bottom and proceeding to 60 s at the top). Red, yellow, green, and aqua bars represent episodes of swimming at speeds ranging from 1 to 3 mm/s, whereas blue bars (speeds below 0.7 mm/s) represent episodes of idling. The darkest blue background represents quiescence. Note that relative to controls the incidence of blue bars is substantially lower during exposure to dopamine or noradrenaline, and substantially higher after treatment with 6-OHDA or TH knockdown.

(B) Quantification of activity episodes registered by visual inspection as swimming (I) or idling (II) under the indicated experimental conditions. Sample sizes in (I) indicate numbers of animals pooled from two batches.

(C) Quantification of the mean speed of overall forward propulsion over an entire recording session under the indicated experimental conditions. *$p < 0.05$; **$p < 0.01$; ***$p < 0.001$. Statistical tests: Mann-Whitney U-test and Kruskal-Wallis ANOVA followed by post hoc Dunn's test.

(B and C) Box and whisker plots show mean (small square within box), median (horizontal line within box), lower and upper quartiles (lower and upper box limits), maximum and minimum (upper and lower limits of whiskers), and outliers (points above or below whiskers).

See also Figure S7 and Videos S3, S4, S5, and S6.

the recording period (1.12 ± 0.28 mm/s compared with 0.79 ± 0.22 mm/s in controls, Figure 5C).

Exposure to exogenous noradrenaline (50 µM) had a similar effect on idling (Figures 3C, 5A, and 5B; Video S4). Idling episodes were substantially less frequent (Figures 5AIII and 5BII), and average total time spent idling decreased, while the duration of quiescent episodes increased about as much as for dopamine exposure (Figure 3C). However, noradrenaline did not increase significantly the forward velocity during swimming (1.81 ± 0.54 mm/s compared with 1.65 ± 0.35 mm/s in controls) nor the overall mean speed of forward propulsion during the recording period (0.99 ± 0.36 mm/s compared with 0.79 ± 0.22 mm/s in controls, Figure 5C).

Pharmacological disruption of dopaminergic synaptic terminals and TH RNA knockdown decrease overall locomotor efficiency

6-hydroxydopamine (6-OHDA) is a neurotoxin that is taken up by dopaminergic synaptic terminals, where its oxidation leads to terminal disruption, loss of dopamine release, and potentially apoptosis of the dopaminergic neurons.[11–13] Exposure to 5 µM 6-OHDA during embryonic development produced a clear behavioral phenotype in the mature animal (Figures 3 and 5; Video S5). As for dopamine augmentation, the incidence of swimming episodes did not change (Figure 5BI). In contrast to dopamine augmentation, the number of idling episodes significantly increased at the expense of quiescence (Figures 3D,

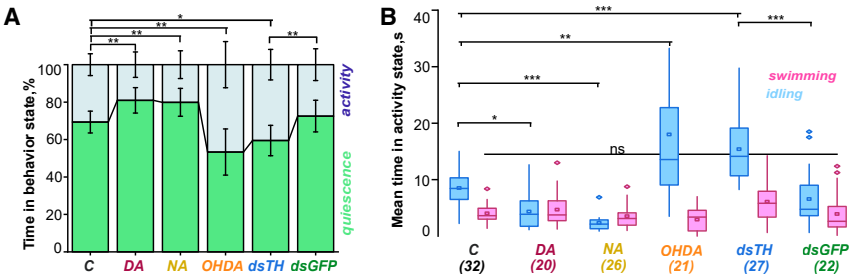

Figure 6. Fraction of time spent in different behavioral states under different experimental conditions

(A) Fraction of time spent in quiescence and activity states under the indicated experimental conditions. Bar height indicates mean, and error bars indicate standard deviation.

(B) Mean time spent in swimming and idling states per minute of recording time under the indicated experimental conditions. *p < 0.05; **p < 0.01; ***p < 0.001. Sample sizes shown below the conditions in (B) represent numbers of animals from two batches. Statistical test: Kruskal-Wallis ANOVA followed by post hoc Dunn's test. Box and whisker plots show mean (small square within box), median (horizontal line within box), lower and upper quartiles (lower and upper box limits), maximum and minimum (upper and lower limits of whiskers), and outliers (points above or below whiskers).

See also Figure S7 and Videos S3, S4, S5, and S6.

5AIV, and 5BII) and thus significantly decreased the overall mean speed of forward propulsion during the recording session (0.43 ± 0.12 mm/s; Figure 5C). The effect was essentially reversed by application of 50 μM dopamine (Figures 5A–5C; Video S5).

Since the effects of 6-OHDA may not be absolutely specific to dopaminergic terminals, we also disrupted dopamine synthesis by knocking down Od-TH gene expression, which was achieved by injecting Od-TH double-stranded RNA (dsRNA) into oocytes prior to fertilization.[33] Injection of dsRNA for GFP was used as a control. qPCR and *in situ* hybridization for Od-TH confirmed efficient knockdown of Od-TH mRNA expression (Figure S7).

Od-TH dsRNA injection produced a behavioral phenotype in the mature animal similar to 6-OHDA exposure, albeit less severe (Figures 3E, 5AVI, and 5BII; Video S6). Od-TH knockdown significantly increased the number of idling episodes at the expense of quiescence and significantly decreased the overall mean speed of forward propulsion relative to the control group (GFP dsRNA injection) (Figures 3E, 3F, and 5C; Video S6).

Locomotor efficiency versus overall activity

Increasing or decreasing dopamine had little effect on the incidence of individual swimming episodes (Figure 5B). The principle effects were on swimming cycle frequency and average forward velocity of individual swimming episodes (shifted toward higher cycle frequencies and velocities with increased dopamine) and particularly on the incidence of idling episodes, which was inversely related to dopamine availability. Since idling comprises a series of bending behaviors, and bending is often exhibited as a prequel or warm-up to swimming in younger animals,[20] one interpretation is that increasing dopamine leads to a more efficient initiation of swimming, whereas decreasing dopamine hampers the initiation of swimming, so that a greater proportion of attempts do not get past the bending phase. In the context of forward propulsion, this can be considered a form of locomotor hypokinesia.

Surprisingly, we found that the overall time in activity, that is, time spent swimming plus time spent idling, was inversely related to dopamine availability (Figure 6). In other words, *Oikopleura* made fewer attempts to move when dopamine levels were elevated, but each attempt led to a more efficient form of movement in the context of forward propulsion (swimming). By contrast, when dopamine levels were diminished, more attempts to move were made, but a greater proportion was less efficient (idling). In humans, dopamine is involved in a number of functions and disease states, including some in which effects on movement may be secondary to mood or impulse, such as anxiety and obsessive-compulsive disorder.[34] *Oikopleura* may therefore be exhibiting a combined phenotype in the face of experimental changes in dopamine, with efficiency of locomotor initiation (hypo- versus hyperkinesia) being one aspect and compulsion to move (time spent in activity) being another.

DISCUSSION

In summary (Figure 7), we have shown that the key elements of locomotor control in *Oikopleura* include a single pair of dopaminergic neurons that can regulate motor output through a small number of interconnected inhibitory GABAergic neurons that comprise a disinhibitory projection upstream of the locomotor CPG. In a bilaterally symmetrical animal, two dopaminergic neurons are the absolute minimum and are substantially fewer than the 13–14 found in *Ciona*.[26,30] In *Ciona*, moreover, based on developmental patterning studies, the dopaminergic neurons have been proposed to reside in the homolog of the vertebrate hypothalamus and photoreceptor field of the retina,[35] rather than the homolog of the vertebrate substantia nigra, and appear to mediate primarily the photic (shadow) response (light-off-induced high-speed swimming).[26] This difference between the appendicularian (*Oikopleura*) and ascidian (*Ciona*) urochordate lineages is not surprising on two grounds. First, *Oikopleura* has no eye and thus no photic response. Second, *Ciona* begins to metamorphose from a motile larva to a sessile adult within about a half day and may not require a motor regulatory system that enables more complex behavioral transitions during its transient larval life. By contrast, *Oikopleura* remains free-swimming throughout life and exhibits a broader repertoire of cardinal movement types,[20] for which behavioral transitions would be facilitated by the presence of a basal ganglia-like function.

Functional identity and expression pattern of the *Oikopleura* dopamine receptor

Previously, the only putative catecholamine receptors identified at the molecular level in a urochordate were the four adrenergic-like receptors (denoted by the abbreviation ADR, which is also used to denote bona fide adrenergic receptors in vertebrates) in *Ciona*, two of which (CiADRb-a and CiADRb-b) have sequence similarity to bilaterian β-ADRs and two of which (CiADRa2-a and CiADRa2-b) have sequence similarity to bilaterian α2-ADRs.[26]

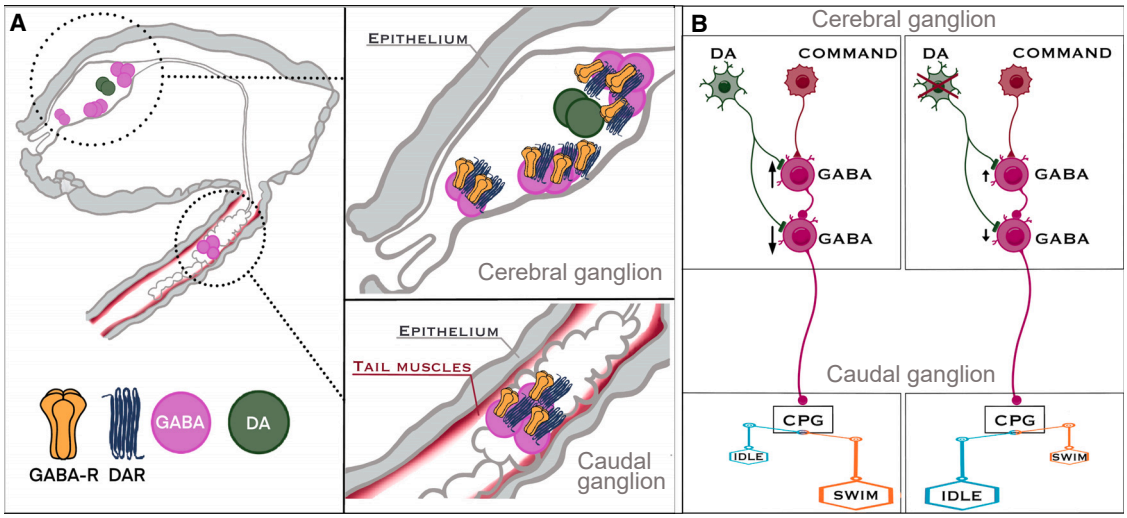

Figure 7. Schematic diagram of the presumed neuronal circuit regulating locomotion in *Oikopleura*

(A) Anatomical location of dopaminergic neurons (DA) and their target Od-DAR-expressing GABAergic neurons (GABA). Note that most GABAergic neurons also express GABA receptors (GABA-R), indicating that there are GABAergic synapses on GABAergic neurons, consistent with disinhibitory connections.

(B) The resultant circuit interactions lead to a dopamine-dependent regulation of the output of movement command signals (COMMAND), regulating the balance between idling and swimming states. Arrows indicate sequential increase or decrease in activity, and the size of arrows represents magnitude.

Only one of these, CiADRa2-a, is expressed in the *Ciona* CNS, and application of an α2-ADR agonist in *Ciona* mimics behavioral responses to elevated dopamine levels.[26] As in *Ciona*, we found no sequences in *Oikopleura* with substantial resemblance to bilaterian dopamine receptors, so we used the predicted CiADRa2-a protein sequence to search for potential catecholamine receptors in *Oikopleura*.

Catecholamine receptors are promiscuous, and both dopamine receptors and ADRs can bind adrenaline, noradrenaline, and dopamine with varying affinities and activate overlapping second messenger systems postsynaptically.[36] Since neither gene sequence nor protein sequence can predict ligand binding unambiguously, we performed a cell-based ligand-binding assay to test the functional identity of the receptor we found in *Oikopleura*. Not surprisingly, responses were obtained on exposure to either dopamine or noradrenaline. However, because our maximum likelihood tree suggests a closer phylogenetic relationship to the vertebrate DRD2 protein than to either the *Ciona* or the vertebrate ADR proteins, we have opted to name this receptor the Od-DAR.

A striking feature influencing our view of the function of dopamine in *Oikopleura* is the specificity of Od-DAR expression by neurons likely to utilize classical neurotransmitters. We found no evidence of Od-DAR expression by putative glutamatergic or cholinergic neurons, only by putative GABAergic neurons, in addition to 5 neurons of unknown neurotransmitter phenotype in the rostral region of the cerebral ganglion. Moreover, all putative GABAergic neurons in the cerebral ganglion (n = 8) and caudal ganglion (n = 3) express Od-DAR, indicating a particularly strong link between dopaminergic signaling and inhibitory circuits (as is the case in vertebrates). This contrasts with the situation in *Ciona* in which CiADRa2-a transcripts are expressed by both putative GABAergic and putative glutamatergic neurons (but not putative cholinergic neurons).[35]

Oikopleura contains a disinhibitory projection to the locomotor CPG

The effect of dopamine in *Ciona* on visuomotor responses and the expression of CiADRa2-a transcripts by both putative glutamatergic and putative GABAergic neurons suggest a dual modulation of *Ciona* swimming behavior: through a disinhibitory visuomotor pathway from GABAergic photoreceptors to GABAergic interneurons to cholinergic premotor interneurons, which mediates the photic response,[31] and through an additional glutamatergic pathway. In *Oikopleura*, there are no photoreceptors, so the inhibitory circuitry affected by dopamine is entirely composed of interneurons. As we have noted, behavioral experiments indicate that there must be a disinhibitory input to the locomotor CPG in the caudal ganglion.[20] This is supported by the expression of GABA-Rs by all putative GABAergic neurons (results reported here), the presence of GABA-positive axons in the connecting nerve[32] and our experiments showing that continuous swimming or bending exhibited by isolated tails is rapidly quelled by exposure to GABA.

A connectome for *Oikopleura* is not yet available (but is underway), so we cannot yet corroborate the disinhibitory projection deduced from these experiments in terms of identified synaptic contacts. Nevertheless, the fact that *Ciona* contains a disinhibitory visuomotor projection,[31] along with the combined evidence described above, suggests strongly that *Oikopleura* also employs a disinhibitory circuit to release locomotion when behaviorally appropriate.

Could the Od-DAR-expressing rostral neurons of unknown neurotransmitter phenotype also contribute to motor regulation? These neurons are evidently neither glutamatergic, GABAergic, or cholinergic (nor glycinergic, since they are not glycine-immunoreactive; A. Trentani and J.C.G., unpublished data). Currently, there is little information available about other potential neurotransmitter phenotypes in that region of the cerebral ganglion, although some neurons there may be peptidergic (A. Trentani

and J.C.G., unpublished data). Nor is there any information available about the effects of other potential neurotransmitters, including peptides, on locomotion. On comparative anatomical grounds, these neurons are unlikely to be among those that project to the caudal ganglion, since in *Ciona* neurons that project from the brain vesicle to the motor ganglion (equivalent respectively to the cerebral and caudal ganglia of *Oikopleura*) are located primarily in the caudal part of the brain vesicle,[30] a situation that is likely to pertain also in *Oikopleura*.[37] Nevertheless, they could be involved in motor-related synaptic connections within the cerebral ganglion.

The putative GABAergic neurons that we have identified in the cerebral ganglion are distributed in three groups, 2 at the very rostral aspect, 3 at the very caudal aspect, and 3 at an intermediate location near the statocyst. These numbers and their spatial distribution correspond perfectly with a prior description[38] at the corresponding stages. The most rostral 2 neurons eventually migrate into the first brain nerves[38] and are likely to be involved in the oral chemosensation that is mediated by those nerves. The most caudal 3 neurons likely provide the descending inhibition to the CPG in the caudal ganglion, as noted above (we note further that prior behavioral experiments on isolated tails suggest the presence of at least two and potentially 3 descending inhibitory pathways from the cerebral to the caudal ganglion[20]). The intermediate 3 neurons are therefore strong candidates for mediating the first inhibitory leg of the disinhibitory pathway that releases swimming and bending behavior. Evidently, both legs of this pathway are subject to modulation by dopamine, since all the putative GABAergic neurons express Od-DAR (Figure 7).

Locomotor efficiency versus behavioral choice?

One interpretation of the differential bias between swimming and idling that arises when dopamine levels are elevated or diminished is that locomotor efficiency depends on sufficiently strong dopaminergic signaling. The relevance to locomotor efficiency is based both on the increase in swimming cycle frequency and velocity seen with elevated dopamine and on the direct relationship between dopamine levels and overall forward propulsion, due to the impairment of forward trajectory that occurs during idling. Moreover, in premetamorphic *Oikopleura*, the bending behavior that comprises idling is an obligatory prequel to the initiation of swimming,[20] and bending alone could therefore be considered as an aborted attempt to initiate swimming. However, bending as warm-up to swimming is down-regulated with development and uncommon in adult animals.[20] An alternative interpretation is that idling and swimming are alternative behaviors with specific purposes and that dopamine availability biases the decision to engage in one versus the other. The purpose of idling remains unclear in this case, but that does not detract from the validity of this interpretation. Since a principal function of the vertebrate nigropallidostriatal system is a context-dependent selection of motor output, both interpretations are consistent with a functional homology between the dopamine-regulated disinhibitory projection in *Oikopleura* and vertebrate basal ganglia circuitry.

Nervous system miniaturization accentuates essential features of motor circuits

As the sister clade to vertebrates and with highly miniaturized nervous systems, urochordates represent a unique platform for revealing highly conserved, core elements of chordate brain circuitry. *Oikopleura*, with even fewer neurons, a less derived (non-sessile) adult lifestyle, and a much broader behavioral repertoire than *Ciona*,[20] is particularly relevant in this context. *Oikopleura* contains one motoneuron per muscle cell,[39] less than a dozen putative GABAergic interneurons,[38] and as we have shown here, only two putative dopaminergic neurons. Within its caudal ganglion, with only about 25 neurons in total (of which 6 are motoneurons), resides the locomotor CPG.[20] The similarity of *Oikopleura*'s dopamine-dependent, disinhibitory motor regulatory system to the vertebrate nigrostriatopallidal system suggests that evolutionary miniaturization in *Oikopleura* has approached a core version of the latter and potentially the minimal circuit necessary to sustain locomotor regulation and context-dependent behavioral selection.

Evolutionary perspective

These findings place the evolution of a dopamine-modulated disinhibitory projection that regulates motor output, similar and likely homologous to the vertebrate nigrostriatopallidal system, at or before the emergence of vertebrates. This type of motor regulatory system has thus been conserved not only throughout the diversification of the vertebrate clade[16] but also through the approximately 600 million years of independent evolution in the urochordate *Oikopleura*. Whether the underlying circuitry and its constituent dopaminergic and GABAergic neurons are truly homologous in *Oikopleura* and vertebrates remains to be determined. That it has survived the extreme miniaturization of the *Oikopleura* nervous system underscores in any case its central importance and adaptive advantage in the control of movement.

STAR★METHODS

Detailed methods are provided in the online version of this paper and include the following:

- KEY RESOURCES TABLE
- RESOURCE AVAILABILITY
  - Lead contact
  - Materials availability
  - Data and code availability
- EXPERIMENTAL MODEL AND STUDY PARTICIPANT DETAILS
  - Animal culture and handling
- METHOD DETAILS
  - Gene cloning
  - Probe synthesis and in situ hybridization (ISH)
  - Synthesis of inhibitory dsRNA for TH and GFP
  - Quantitative real-time PCR (qPCR)
  - Gene knockdown analysis using qPCR
  - Microinjection
  - Phylogenetics
  - 5' and 3' RACE
  - Imaging
  - Heterologous expression studies
  - Calcium imaging
  - Behavioral assessment
  - Pharmacological manipulations
- QUANTIFICATION AND STATISTICAL ANALYSIS

- Colocalization analysis
- Calcium imaging video analysis
- Behavioral video analysis
- Statistics

SUPPLEMENTAL INFORMATION

Supplemental information can be found online at https://doi.org/10.1016/j.cub.2023.08.015.

ACKNOWLEDGMENTS

Norwegian Research Council grant 234817 (to the Sars International Centre for Marine Molecular Biology, University of Bergen), and intramural grants from the Institute of Basic Medical Sciences, University of Oslo (to J.C.G.). We gratefully acknowledge the staff of the Sars Centre Oikopleura Facility, especially Anne Elin Aasjord, for the provision of animals, and we thank Keith Sillar, John Simmers, and Sten Grillner for critical comments on an earlier version of the manuscript.

AUTHOR CONTRIBUTIONS

Conceptualization, J.C.G., O.T., and Y.M.; methodology, O.T., Y.M., and J.C.G.; investigation, O.T., Y.M., and J.C.G.; visualization, O.T. and Y.M.; funding acquisition, J.C.G.; project administration and supervision, J.C.G.; and writing – original draft, subsequent review, and editing, J.C.G., O.T., and Y.M.

DECLARATION OF INTERESTS

The authors declare no competing interests.

INCLUSION AND DIVERSITY

We support inclusive, diverse, and equitable conduct of research.

Received: December 21, 2022
Revised: June 14, 2023
Accepted: August 3, 2023
Published: August 28, 2023

REFERENCES

1. Farries, M.A. (2013). How 'basal' are the basal ganglia? Commentary on Strausfeld NJ and Hirth F (2013a): Deep homology of arthropod central complex and vertebrate basal ganglia. Science 340: 157-161. Brain Behav. Evol. *82*, 211–214.
2. Strausfeld, N.J., and Hirth, F. (2013). Homology versus convergence in resolving transphyletic correspondences of brain organization. Brain Behav. Evol. *82*, 215–219.
3. Bennett, M.S. (2021). Five breakthroughs: a first approximation of brain evolution from early bilaterians to humans. Front. Neuroanat. *15*, 693346.
4. Glover, J.C. (2020). Oikopleura. Curr. Biol. *30*, R1243–R1245.
5. Delsuc, F., Brinkmann, H., Chourrout, D., and Philippe, H. (2006). Tunicates and not cephalochordates are the closest living relatives of vertebrates. Nature *439*, 965–968.
6. Seo, H.C., Kube, M., Edvardsen, R.B., Jensen, M.F., Beck, A., Spriet, E., Gorsky, G., Thompson, E.M., Lehrach, H., Reinhardt, R., and Chourrout, D. (2001). Miniature genome in the marine chordate *Oikopleura dioica*. Science *294*, 2506.
7. Søviknes, A.M., and Glover, J.C. (2007). Spatiotemporal patterns of neurogenesis in the appendicularian Oikopleura dioica. Dev. Biol. *311*, 264–275.
8. Obeso, J.A., Rodríguez-Oroz, M.C., Benitez-Temino, B., Blesa, F.J., Guridi, J., Marin, C., and Rodriguez, M. (2008). Functional organization of the basal ganglia: therapeutic implications for Parkinson's disease. Mov. Disord. *23*, S548–S559.
9. Archer, T., and Fredriksson, A. (2003). An antihypokinesic action of alpha2-adrenoceptors upon MPTP-induced behaviour deficits in mice. J. Neural Transm. (Vienna) *110*, 183–200.
10. Hara, M., Fukui, R., Hieda, E., Kuroiwa, M., Bateup, H.S., Kano, T., Greengard, P., and Nishi, A. (2010). Role of adrenoceptors in the regulation of dopamine/DARPP-32 signaling in neostriatal neurons. J. Neurochem. *113*, 1046–1059.
11. Dauer, W., and Przedborski, S. (2003). Parkinson's disease: mechanisms and models. Neuron *39*, 889–909.
12. Simola, N., Morelli, M., and Carta, A.R. (2007). The 6-hydroxydopamine model of Parkinson's disease. Neurotox. Res. *11*, 151–167.
13. Hernandez-Baltazar, D., Zavala-Flores, L.M., and Villanueva-Olivo, A. (2017). The 6-hydroxydopamine model and parkinsonian pathophysiology: novel findings in an older model. Neurologia *32*, 533–539.
14. Zesiewicz, T.A., and Sullivan, K.L. (2011). Drug-induced hyperkinetic movement disorders by nonneuroleptic agents. Handb. Clin. Neurol. *100*, 347–363.
15. Wullimann, M.F. (2014). Ancestry of basal ganglia circuits: new evidence in teleosts. J. Comp. Neurol. *522*, 2013–2018.
16. Grillner, S. (2021). Evolution of the vertebrate motor system - from forebrain to spinal cord. Curr. Opin. Neurobiol. *71*, 11–18.
17. Strausfeld, N.J., and Hirth, F. (2013). Deep homology of arthropod central complex and vertebrate basal ganglia. Science *340*, 157–161.
18. Athira, A., Dondorp, D., Rudolf, J., Peytral, O., and Chatzigeorgiou, M. (2022). Comprehensive analysis of locomotion dynamics in the protochordate *Ciona intestinalis* reveals how neuromodulators flexibly shape its behavioral repertoire. PLoS Biol. *20*, e3001744.
19. Barron, A.B., Søvik, E., and Cornish, J.L. (2010). The roles of dopamine and related compounds in reward-seeking behavior across animal phyla. Front. Behav. Neurosci. *4*, 163.
20. Kreneisz, O., and Glover, J.C. (2015). Developmental characterization of tail movements in the appendicularian urochordate *Oikopleura dioica*. Brain Behav. Evol. *86*, 191–209.
21. Bouquet, J.-M., Spriet, E., Troedsson, C., Otterå, H., Chourrout, D., and Thompson, E.M. (2009). Culture optimization for the emergent zooplanktonic model organism *Oikopleura dioica*. J. Plankton Res. *31*, 359–370.
22. Walker, S.J., Liu, X., Roskoski, R., and Vrana, K.E. (1994). Catalytic core of rat tyrosine hydroxylase: terminal deletion analysis of bacterially expressed enzyme. Biochim. Biophys. Acta *1206*, 113–119.
23. Bezem, M.T., Baumann, A., Skjærven, L., Meyer, R., Kursula, P., Martinez, A., and Flydal, M.I. (2016). Stable preparations of tyrosine hydroxylase provide the solution structure of the full-length enzyme. Sci. Rep. *6*, 30390.
24. Goodwill, K.E., Sabatier, C., and Stevens, R.C. (1998). Crystal structure of tyrosine hydroxylase with bound cofactor analogue and iron at 2.3 Å resolution: self-hydroxylation of Phe300 and the pterin-binding site. Biochemistry *37*, 13437–13445.
25. Kelley, L.A., Mezulis, S., Yates, C.M., Wass, M.N., and Sternberg, M.J. (2015). The Phyre2 web portal for protein modeling, prediction and analysis. Nat. Protoc. *10*, 845–858.
26. Razy-Krajka, F., Brown, E.R., Horie, T., Callebert, J., Sasakura, Y., Joly, J.S., Kusakabe, T.G., and Vernier, P. (2012). Monoaminergic modulation of photoreception in ascidian: evidence for a proto-hypothalamo-retinal territory. BMC Biol. *10*, 45.
27. Cañestro, C., Bassham, S., and Postlethwait, J. (2005). Development of the central nervous system in the larvacean *Oikopleura dioica* and the evolution of the chordate brain. Dev. Biol. *285*, 298–315.
28. Kamesh, N., Aradhyam, G.K., and Manoj, N. (2008). The repertoire of G protein-coupled receptors in the sea squirt *Ciona intestinalis*. BMC Evol. Biol. *8*, 129.
29. de Souza, J.F., de Mello, A.A., Portal, T.M., Nunes-da-Fonseca, R., and Monteiro de Barros, C. (2021). Novel insights about the ascidian dopamine system: pharmacology and phylogenetics of catecholaminergic receptors on the *Phallusia nigra* immune cells. Fish Shellfish Immunol. *109*, 41–50.

30. Ryan, K., Lu, Z., and Meinertzhagen, I.A. (2016). The CNS connectome of a tadpole larva of *Ciona intestinalis* (L.) highlights sidedness in the brain of a chordate sibling. ELife *5*, e16962.

31. Kourakis, M.J., Borba, C., Zhang, A., Newman-Smith, E., Salas, P., Manjunath, B., and Smith, W.C. (2019). Parallel visual circuitry in a basal chordate. ELife *8*, e44753.

32. Bollner, T., Storm-Mathisen, J., and Ottersen, O.P. (1991). GABA-like immunoreactivity in the nervous system of *Oikopleura dioica* (Appendicularia). Biol. Bull. *180*, 119–124.

33. Mikhaleva, Y., Kreneisz, O., Olsen, L.C., Glover, J.C., and Chourrout, D. (2015). Modification of the larval swimming behavior in *Oikopleura dioica*, a chordate with a miniaturized central nervous system by dsRNA injection into fertilized eggs. J. Exp. Zool. B Mol. Dev. Evol. *324*, 114–127.

34. Stein, D.J. (2002). Obsessive-compulsive disorder. Lancet *360*, 397–405.

35. Moret, F., Christiaen, L., Deyts, C., Blin, M., Joly, J.-S., and Vernier, P. (2005). The dopamine-synthesizing cells in the swimming larva of the tunicate *Ciona intestinalis* are located only in the hypothalamus-related domain of the sensory vesicle. Eur. J. Neurosci. *21*, 3043–3055.

36. Ranjbar-Slamloo, Y., and Fazlali, Z. (2020). Dopamine and noradrenaline in the brain; overlapping or dissociate functions? Front. Mol. Neurosci. *12*, 334.

37. Holmberg, K. (1984). A transmission electron microscopic investigation of the sensory vesicle in the brain of *Oikopleura dioica* (Appendicularia). Zoomorphology *104*, 298–303.

38. Søviknes, A.M., Chourrout, D., and Glover, J.C. (2005). Development of putative GABAergic neurons in the appendicularian urochordate *Oikopleura dioica*. J. Comp. Neurol. *490*, 12–28.

39. Søviknes, A.M., Chourrout, D., and Glover, J.C. (2007). Development of the caudal nerve cord, motoneurons, and muscle innervation in the appendicularian urochordate *Oikopleura dioica*. J. Comp. Neurol. *503*, 224–243.

40. Katoh, K., and Standley, D.M. (2013). MAFFT multiple sequence alignment software version 7: improvements in performance and usability. Mol. Biol. Evol. *30*, 772–780.

41. Waterhouse, A.M., Procter, J.B., Martin, D.M.A., Clamp, M., and Barton, G.J. (2009). Jalview version 2--a multiple sequence alignment editor and analysis workbench. Bioinformatics *25*, 1189–1191.

42. Kalyaanamoorthy, S., Minh, B.Q., Wong, T.K.F., von Haeseler, A., and Jermiin, L.S. (2017). ModelFinder: fast model selection for accurate phylogenetic estimates. Nat. Methods *14*, 587–589.

43. Rambaut, A.. FigTree v. 1.4.4. http://tree.bio.ed.ac.uk/software/figtree/.

44. Rodriguez, A., Zhang, H., Klaminder, J., Brodin, T., Andersson, P.L., and Andersson, M. (2018). ToxTrac: a fast and robust software for tracking organisms. Methods Ecol. Evol. *9*, 460–464.

45. Asencio, C., Rodríguez-Aguilera, J.C., Ruiz-Ferrer, M., Vela, J., and Navas, P. (2003). Silencing of ubiquinone biosynthesis genes extends life span in *Caenorhabditis elegans*. FASEB J. *17*, 1135–1137.

46. Mikhaleva, Y., Tolstenkov, O., and Glover, J.C. (2019). Gap junction-dependent coordination of intercellular calcium signalling in the developing appendicularian tunicate *Oikopleura dioica*. Dev. Biol. *450*, 9–22.

47. Pfaffl, M.W. (2001). A new mathematical model for relative quantification in real-time RT-PCR. Nucleic Acids Res. *29*, e45.

48. Hoang, D.T., Chernomor, O., Von Haeseler, A., Minh, B.Q., and Vinh, L.S. (2018). UFBoot2: improving the ultrafast bootstrap approximation. Mol. Biol. Evol. *35*, 518–522.

49. Minh, B.Q., Schmidt, H.A., Chernomor, O., Schrempf, D., Woodhams, M.D., von Haeseler, A., and Lanfear, R. (2020). IQ-TREE 2: new models and efficient methods for phylogenetic inference in the genomic era. Mol. Biol. Evol. *37*, 1530–1534.

50. Bolte, S., and Cordelières, F.P. (2006). A guided tour into subcellular colocalization analysis in light microscopy. J. Microsc. *224*, 213–232.

51. Costes, S.V., Daelemans, D., Cho, E.H., Dobbin, Z., Pavlakis, G., and Lockett, S. (2004). Automatic and quantitative measurement of protein-protein colocalization in live cells. Biophys. J. *86*, 3993–4003.

52. Rudolf, J., Dondorp, D., Canon, L., Tieo, S., and Chatzigeorgiou, M. (2019). Automated behavioural analysis reveals the basic behavioural repertoire of the urochordate *Ciona intestinalis*. Sci. Rep. *9*, 2416.

STAR★METHODS

KEY RESOURCES TABLE

REAGENT or RESOURCE	SOURCE	IDENTIFIER
Bacterial and virus strains		
One Shot™ TOP10 Chemically Competent *E. coli*	ThermoFisher	Cat# C4040-10
Chemicals, peptides, and recombinant proteins		
SuperScript IV Reverse Transcriptase	ThermoFisher	Cat# 18090010
BioTaq DNA polymerase	Bioline	Cat# BIO-21040
iQ SYBR Green Supermix	Bio-Rad	Cat# 1708880
Lipofectamine 3000 Reagent	Invitrogen	Cat# L3000015
Fluo-4AM	Fisher Scientific	Cat# F-14201
dopamine hydrochloride	Sigma-Aldrich	Cat# H-8502, CAS: 62-31-7
noradrenaline hydrochloride	Sigma-Aldrich	Cat# A-7256, CAS: 55-27-6
6-hydroxydopamine hydrochloride	Sigma-Aldrich	Cat# H-4381, CAS: 28094-15-7
Critical commercial assays		
NucleoSpin® RNA XS	Macherey-Nagel	Cat# 740902.50
QIAquick Gel Extraction Kit	Qiagen	Cat# 28706
QIAprep Spin Miniprep Kit	Qiagen	Cat# 27104
BigDye™ Terminator v3.1 Cycle Sequencing Kit	ThermoFisher	Cat# 4337455
T4 ligase kit	Promega	Cat# M1801
Experimental models: Cell lines		
HEK-293	ATCC	CRL-1573
Experimental models: Organisms/strains		
Oikopleura dioica	Michael Sars Centre *Oikopleura* Facility	www.uib.no/en/michaelsarscentre/114926/appendicularian-facility
Oligonucleotides		
TH2 (f1) TAAGACGGCAGAGCACTCTTGTAC	This paper	GenBank: CBY12061.1
TH2 (r2) GAGGATGATCAGGCTCGTCAGTAACA	This paper	GenBank: CBY12061.1
Od-DAR (f3) GATGACGATTCTGGCATTCTACCGTT	This paper	GenBank: CBY09491.1, CBY37057.1
Od-DAR (r2) TGTCCTTCTCAGTGTCGCTCGAAT	This paper	GenBank: CBY09491.1, CBY37057.1
VGluT (f1) AGGAGTCAAAATGGAAGTTCTT	This paper	GenBank: CBY10417.1
VGluT (r2) TGTGAAGCGTCTAGATTTAGAAC	This paper	GenBank: CBY10417.1
AADC (f2) TTGTACCGTCGCCAATCCAGTAAAG	This paper	GenBank: CBY20168.1
AADC (r1) CCAAATGCAAGCGTCCAGTCAC	This paper	GenBank: CBY20168.1
MOXD1(DBH) (f1) TTGGAATCGGAATAAACAGGCG	This paper	GenBank: CBY11687.1
MOXD1 (DBH) (r1) ACGGAAATGTGGCCAGCTTCAT	This paper	GenBank: CBY11687.1
GABA-Rα6 (f1): GCGACCTTGGACTCAATTTTAC	This paper	GenBank: CBY20019.1; CBY33125.1
GABA-Rα6 (r3e-i): CCTCAATCGTGTAACCGTATGAGC	This paper	GenBank: CBY20019.1; CBY33125.1
qPCR-TH (Fe-i) AATCGCAAAAGCCAGGTCGCAAGT	This paper	N/A
qPCR-TH (Re-i) TCGGTAGATTCCTCGAGGACG	This paper	N/A
qPCR- Od-DAR (R6e-i) CTGAAAGGTGCAGCTGAAGTGAT	This paper	N/A
OT1 (F) GACGCCCGTCATCAAATCGCAA	This paper	N/A
OT2 (R) CCTGAGTTGTTGAAACATCGTCC	This paper	N/A
Od-DAR -5race(R) GATTACGCCAAGCTTTTCTCAGTGTC GCTCGAATGCTT	This paper	N/A
Od-DAR -5race(n-R) GATTACGCCAAGCTTTTGTACGTC GCCATCTGTTCTTC	This paper	N/A
Od-DAR -3race(F) GATTACGCCAAGCTTGATCACTTCA GCTGCACCTTTCAG	This paper	N/A

(*Continued on next page*)

Continued

REAGENT or RESOURCE	SOURCE	IDENTIFIER
Od-DAR -3race(n-F) GATTACGCCAAGCTTCTGCGGCTA TACTTCAATTGTGTG	This paper	N/A
Recombinant DNA		
pp2A-mCherry-N1 vector	Addgene (gift from Dorus Gadella)	plasmid #84329
Gna15 (NM_010304) Mouse Tagged ORF Clone	Origene	Cat# MR205807
pGem-T-Easy Vector	Promega	Cat# A1360
Software and algorithms		
IDT OligoAnalyzer 3.1 webtool	https://eu.idtdna.com/	N/A
BLASTp	NCBI	N/A
MAFFT	https://mafft.cbrc.jp/alignment/server/	N/A
L-INS-I	Katoh and Standley[40]	N/A
Jalview 2	Waterhouse et al.[41]	N/A
ModelFinder, IQ-TREE	Kalyaanamoorthy et al.[42]	N/A
JTT+I+G4 substitution model, IQ-TREE	Kalyaanamoorthy et al.[42]	N/A
FigTree v1.4.4	Rambaut[43]	N/A
NisElements4.2	Nikon	N/A
Bitplane AG	Imaris	N/A
Procreate	Savage Interactive	N/A
WinFluor	Strathclyde University	N/A
Motion Monitor	Rodriguez et al.[44]	N/A
JACoP plugin	ImageJ	N/A
Matlab	MathWorks	N/A
VirtualDub	Rodriguez et al.[44]	N/A
ToxTrac	Rodriguez et al.[44]	N/A
OriginPro 2020	OriginLab	N/A

RESOURCE AVAILABILITY

Lead contact

Further information and requests for resources and reagents should be directed to and will be fulfilled by the lead contact, Joel C. Glover (joel.glover@medisin.uio.no).

Materials availability

Plasmids generated in this study are available on request.

Data and code availability

- All data sets are stored at a central server at the Sars International Centre for Marine Molecular Biology and are available from the lead contact upon request.
- Any additional information required to reanalyze the data reported in this paper is available from the lead contact upon request.

EXPERIMENTAL MODEL AND STUDY PARTICIPANT DETAILS

Animal culture and handling

Oikopleura cultures were maintained in an automated facility at the Sars International Centre for Marine Molecular Biology. Details of controlled *in vitro* spawning are described in[21] and the overall life cycle is shown in Figure S1. To isolate tails for assessment of movement in the absence of descending inputs from the cerebral ganglion (see Video S2), D1 animals were subjected to trituration through a Pasteur pipette until tails had separated from the heads.

METHOD DETAILS

Gene cloning

The following gene-specific primers were designed for Od-TH (GSOIDT00017928001, GenBank: CBY12061.1), Od-DAR (GSOIDT00008492001, GenBank: CBY09491.1, CBY37057.1), VGluT (GSOIDT00012440001, GenBank: CBY10417.1). AADC (GSOIDT00000153001, GenBank: CBY20168.1), MOXD1 (monooxygenase DBH-like 1) (GSOIDG00016864001, GenBank: CBY11687.1), GABA-R-alpha6 (GSOIDT00000001001, GenBank: CBY20019.1; CBY33125.1):

- TH2 (f1) TAAGACGGCAGAGCACTCTTGTAC
- TH2 (r2) GAGGATGATCAGGCTCGTCAGTAACA
- Od-DAR (f3) GATGACGATTCTGGCATTCTACCGTT
- Od-DAR (r2) TGTCCTTCTCAGTGTCGCTCGAAT
- VGluT (f1) AGGAGTCAAAATGGAAGTTCTT
- VGluT (r2) TGTGAAGCGTCTAGATTTAGAAC
- AADC (f2) TTGTACCGTCGCCAATCCAGTAAAG
- AADC (r1) CCAAATGCAAGCGTCCAGTCAC
- MOXD1(DBH) (f1) TTGGAATCGGAATAAACAGGCG
- MOXD1 (DBH) (r1) ACGGAAATGTGGCCAGCTTCAT
- GABA-Rα6 (f1): GCGACCTTGGACTCAATTTTAC
- GABA-Rα6 (r3e-i): CCTCAATCGTGTAACCGTATGAGC

ChAT (GSOIDT00013449001, GenBank: ABK35121.1), and GAD (GSOIDT00008657001, GenBank: CBY19512.1) genes were previously cloned as described in Mikhaleva et al.[33]

Isolation of total RNA from different developmental stages (5-7 hpf and 10-11 hpf) was performed using NucleoSpin® RNA XS (Macherey-Nagel, AH-diagnostics, Oslo, Norway). First strand cDNA synthesis was performed with SuperScript IV Reverse Transcriptase (ThermoFisher Scientific, Oslo, Norway). A PCR was set up with 2 μl of the first strand reaction in concentration 20 ng/μl as template using 0.5μl of each of the specific primers (10μM). Reaction mix consisted of 2.5 μl NH4+buffer, 10x; 1.5 μl of 2,5mM dNTP; 1.3μl of 50 mM MgCl2; 0.5 μl BioTaq enzyme (Bioline, 5U/μl), 11.5 μl H_2O.

The PCR cycle was used with denaturation at 94°C for 3 min, 35 cycles of 94°C (15 seconds), 65°C-69°C gradient (30 seconds), 68°C (60 seconds), followed by elongation at 68°C for 7 minutes and storage at 4°C. PCR products were electrophoresed on a 1% TAE agarose gel. The expected PCR fragment was identified, and the gel bands were cut out and purified with QIAquick Gel Extraction Kit (Qiagen, Chatsworth, CA). The PCR fragment was ligated into a pGem-T-Easy Vector system (Promega) in a reaction mixture containing 5 μl of 2x ligation buffer, 1 μl of T4 DNA ligase, 1 μl vector (50 ng/μl), and 5 μl of the purified PCR fragment, at 4°C overnight. Transformation was performed into 20μl of One Shot™ TOP10 Chemically Competent *E. coli* (ThermoFisher Scientific, Oslo, Norway) and 1 μl of the ligated PCR fragments in the pGEM T-Easy Vector.

The recombinant bacteria were plated out on LB/amp, X-gal, IPTG agar plates and incubated at 37°C overnight. Three white clones were picked for every gene based on blue-white screening. Colonies were grown in a 5ml of overnight culture in LB medium (shaking at 37°C) with 100 mg/ml ampicillin. Plasmid purification was performed the next day using QIAprep Spin Miniprep Kit (Qiagen). Sequencing reaction was performed for every cloned fragment with BigDye™ Terminator v3.1 Cycle Sequencing Kit (ThermoFisher Scientific, Oslo, Norway) and SP6 and T7 primers.

Probe synthesis and in situ hybridization (ISH)

Cloned sequences inserted into the pGemTeasy vector were used as templates for sense and antisense probe synthesis as described previously.[39] Embryos for *in situ* hybridization (ISH) were collected at different developmental stages (from tailbud to 15 hpf) and fixed with 4%PFA. ISH was performed as described previously.[33,39]

Synthesis of inhibitory dsRNA for TH and GFP

pGemTeasy vector with insertion of the TH sequence (TH(f1)-TH(r2) – 1158bp) was used as a template for PCR amplification with M13(f) and M13(r) primers. Linear DNA fragments of the TH gene were run on a 1% TAE agarose gel, bands were cut out and purified with QIAquick Gel Extraction Kit (Qiagen, Chatsworth, CA). DNA fragments and the L4440 vector were cut with NcoI and SpeI enzymes (NEB) and TH DNA fragments were ligated into the L4440 vector.

An EGFP sequence was cut out from the EGFP-N1 vector with NotI/HindIII enzymes (NEB), as was the L4440 vector, and the EGFP sequence was ligated into the L4440 vector using the T4 ligase kit (Promega).

Transformation of 1.5 μl of the ligated PCR fragments in the L4440 Vector into 20μl of One Shot™ TOP10 Chemically Competent E. coli (C4040-10, ThermoFisher Scientific, Oslo, Norway) was performed. On the next day, six colonies for TH and three colonies for EGFP were picked from agar plates containing 100 mg/ml ampicillin and cultured overnight. Plasmids were purified with Miniprep Kit (Cat No. 27104, Qiagen). Two out of six TH-L4440 minipreps contained the TH-gene insert at a concentration of about 100 ng/μl. All minipreps with EGFP-L4440 plasmid were positive and had plasmid concentrations ranging from 120-130 ng/μl.

2μl of purified plasmids were used for transformation into 100μl of homemade HT115 competent bacteria.[45] After dsRNA was produced in bacterial culture, it was purified as described earlier.[33,46] The final concentration of dsRNA-TH and dsRNA-EGFP in the ddH_2O was 1000 ng/mL.

Quantitative real-time PCR (qPCR)

To obtain expression profiles of TH and DAR genes, total RNA was isolated from embryos starting from the 2-cell stage (1 hpf) and then every hour up to 12 hpf. Total RNA and sscDNA were generated as described above. RT-qPCR was performed using iQ SYBR Green Supermix (Bio-Rad, Oslo, Norway). Primers for qPCR were designed using IDT OligoAnalizer 3.1 webtool. Optimal primer pair was chosen for each gene: qPCR-TH(Fe-i) - qPCR-TH(Re-i) for TH (337bp), and Od-DAR (f3) - qPCR- Od-DAR (R6e-i) (178bp). Primers indicated as e-i were situated at the exon-intron border to eliminate possible contamination from gDNA. Amplification efficiency was determined by generating a standard curve using serial dilutions of a template and gave R2>0.970.

The BioRAD-qPCR Detection System was used for qPCR, with the following cycle: denaturation for 3 min at 95 °C, 39 cycles at 95 °C for 10 sec, 65 °C for 30 sec and 72 °C for 30 sec, with final extension for 30 sec at 55 °C, with a subsequent temperature increase to 95 °C. Expression levels of TH and Od-DAR genes were normalized against RPL23–ribosomal protein gene expression. Differences in mRNA levels between injected and non-injected animals was calculated using the comparative method of relative quantification.[47]

- qPCR-TH (Fe-i) AATCGCAAAAGCCAGGTCGCAAGT
- qPCR-TH (Re-i) TCGGTAGATTCCTCGAGGACG
- qPCR- Od-DAR (R6e-i) CTGAAAGGTGCAGCTGAAGTGAT

Gene knockdown analysis using qPCR

Eggs spawned from 5 females were injected with dsRNA-TH at concentration 1000ng/μl and embryos were allowed to develop until the late larval stage. Total RNA was isolated from 25 injected embryos and 25 control embryos from each female. sscDNA was generated as described above. RT-qPCR was performed with these primer pairs:

- TH gene: OT1 (F) GACGCCCGTCATCAAATCGCAA – OT2 (R) CCTGAGTTGTTGAAACATCGTCC (100 bp).
- Od-DAR gene: Same as for the expression profile.

Microinjection

dsRNA-TH was injected into unfertilized eggs obtained from *in vitro* spawns. Injected eggs were transferred to 6-well cell culture plates (VWR, Oslo, Norway) coated with 1% agarose (Promega, Oslo, Norway), fertilized with 50 μl of sperm solution and incubated in fresh FASW for 24 hours. Preparation of equipment necessary for injections (injection needles, oocyte holding pipettes, FASW and sperm solution) and collection of mature animals were as described previously.[33,46]

Phylogenetics

We performed phylogenetic analyses of α2ADR receptor proteins in tunicates. Full-length protein sequences of α2ADR and D2R2 from tunicates and selected vertebrates were obtained using BLASTp in NCBI or from published articles (See accession numbers in Table S1). Sequences were aligned using MAFFT https://mafft.cbrc.jp/alignment/server/ and L-INS-I[40] and visualized in Jalview 2.[41] The best-fit substitution model for each alignment was determined using the ModelFinder in IQ-TREE.[42] Maximum likelihood analyses using the JTT+I+G4 substitution models for protein evolution were performed in IQ-TREE, with branch supports calculated by 10,000 Ultrafast bootstrap replicates (UFBoot2) from maximum 1000 iterations (stopping rule)[48,49] using the vertebrate 5HT1A receptors as an outgroup. The generated consensus trees were rooted and visualized with FigTree v1.4.4.[43]

5' and 3' RACE

The 5' and 3' end sequences of mRNA from the Od-DAR gene were captured using a standard protocol and the SMARTer RACE cDNA Amplification Kit (634858, TakaraBio, CA, USA). The following primers were used:

- Od-DAR -5race(R) GATTACGCCAAGCTTTTCTCAGTGTCGCTCGAATGCTT
- Od-DAR -5race(n-R) GATTACGCCAAGCTTTTGTACGTCGCCATCTGTTCTTC
- Od-DAR -3race(F) GATTACGCCAAGCTTGATCACTTCAGCTGCACCTTTCAG
- Od-DAR -3race(n-F) GATTACGCCAAGCTTCTGCGGCTATACTTCAATTGTGTG

All obtained bands were cut out of a 1% TAE gel, purified with gel extraction kit and cloned into pGemT-easy vector, then sequenced with SP6 and T7 primers as described above.

Imaging

Non-fluorescent images were acquired with a Nikon Digital Sight DSU3 camera mounted on a Nikon Eclipse E800 compound microscope equipped with a 40x oil immersion objective (numerical aperture 1.00) using differential interference (Nomarski) optics. Acquisition and minor adjustment of contrast and brightness were performed with the NisElements4.2 program.

Fluorescent images were acquired with a Leica SP5 confocal microscope. Imaris software (Bitplane AG) was used for 3D reconstruction of confocal image series.

Images were cropped to an area of interest and any adjustment of brightness and contrast was applied to the entire cropped image, ensuring that no information in the image was lost through saturation or thresholding. Cropped images were resized and figures were composed using the Procreate program (Savage Interactive Pty Ltd.)

Heterologous expression studies

For expression and functional pharmacological analyses of Od-DAR binding, the full-length cDNA of Od-DAR (long) was expressed in mammalian cells. The full-length cDNA was ordered from Gene Universal Inc. with the addition of a NheI (GCTAGC) site at the 5' end and a HindIII (AAGCTT) site at the 3' end. Initially, the gene was cloned into the pcDNA3.1(+)-EGFP vector. Later the full sequence of Od-DAR was subcloned into the pp2A-mCherry-N1 vector (a gift from Dorus Gadella, plasmid #84329, Addgene) using the NheI and HindIII enzymes. This vector enables the bicistronic expression of the protein of interest and mCherry. It was co-transfected with a mouse G-protein expressing vector (Gna15 (NM_010304) Mouse Tagged ORF Clone (MR205807, Origene) to permit signal transduction in HEK293 cells.

HEK293 cells were seeded into 24-well plates in Dulbecco's Modified Essential Media (DMEM) supplemented with 20mM HEPES and 10% heat inactivated fetal calf serum. The following day, cells were transfected using Lipofectamine 3000 Reagent (Invitrogen) according to manufacturer's instructions and allowed to grow overnight. Transfection with the Gna15 vector was the negative control, and co-transfection of Gna15 and a mouse ADR-expressing vector subcloned into the pp2A-mCherry-N1 vector was the positive control. Transfected cells were identified by mCherry expression prior to imaging.

Calcium imaging

Three days post-transfection, HEK293 cells were washed twice in warm Hepes-buffered saline (pH 7.3) and incubated (30 min in the dark) in the same containing 50 μM Fluo-4AM Ca2+ indicator (Fisher Scientific, Oslo, Norway) prior to pharmacological manipulations. After incubation, cells were washed 2x5min with warm Hepes-buffered saline, and positioned under an epifluorescence microscope (Axioscop FS-2 (Zeiss) with a 40x water-immersion objective (LUMPlanF1, 0.8 NA (Olympus) and equipped with a 100 W halogen lamp. A Cascade 650 cooled CCD camera (Photometrics) and WinFluor software (Strathclyde University) were used to record Ca2+ transients. Stock solutions of dopamine hydrochloride or noradrenaline hydrochloride were added after 30 s to reach final concentrations of 50 μM. We recorded Ca2+ transients at 100 fps for 2 min in total. Controls included exposure to Hepes-buffered saline alone and Hepes-buffered saline containing ascorbic acid, exposure to dopamine hydrochloride solution to blank and mock control cells. Heterologous expression and Ca2+ imaging experiments were performed at the Laboratory of Neural Development and Optical Recording (NDEVOR), Department of Molecular Medicine, Institute of Basic Medical Sciences, University of Oslo.

Behavioral assessment

Our behavioral setup was built on the ZEISS Stereo Discovery.V8 stereomicroscope with a Plan Apo S 1x FWD 81 mm lens, a KL 2500 LED (Schott) light source and a dark field condenser Leitz Wetzlar D 0.80 for image contrasting. A custom made aluminum arena (2 mm depth and D 5.2 mm) with cooling Insert UP-Set 2000 (Pecon) adapted for microscopic slides was connected to a Titan (Aqua Medic) water cooling unit. Videos were recorded using the IDT X-Stream 1440p PCIe 2.0 high speed camera (IDT) at 400 fps and Motion Monitor software.

After *in vitro* fertilization, animals were kept at 18 °C overnight. Day 1 animals were stimulated to leave the house prior to recordings by gently poking the house with a hair fastened to a syringe needle prior to recording. For recording, single animals (or isolated tails) were placed in the arena cooled to 18°C and allowed to adapt for 4 min. We recorded one 2-minute video of about 48 000 frames per animal (or isolated tail) for behavioral analysis. At least 20 animals from two different spawns were recorded per experimental condition (control, application of chemicals or after injection of dsRNA).

Pharmacological manipulations

Stock solutions of dopamine hydrochloride, noradrenaline hydrochloride and 6-hydroxydopamine hydrochloride (Sigma, Norway) were made in FASW or HEPES-buffered saline and stored at -20°C. Working solutions (50 microM for behavioral experiments and HEK cell experiments and 5 microM for 6-OHDA pretreatment) were made by dilution of stock solutions in FASW (behavioral experiments and 6-OHDA pretreatment) or HEPES-buffered saline (HEK cell experiments). Behavioral experiments were initiated by placing D1 animals into working solutions of dopamine hydrochloride or noradrenaline hydrochloride in 6-well tissue plates 5 minutes prior to video recording. Control animals were recorded in FASW. 6-OHDA pretreatment involved placing 4 hpf embryos in the working solution and leaving them overnight, and then transferring them to FASW for video recording.

QUANTIFICATION AND STATISTICAL ANALYSIS

Colocalization analysis

Colocalization analysis of different wavelength signals was performed in ImageJ (NIH) using the JACoP plugin.[50] We used pixel intensity spatial correlation analysis and evaluated the intensity correlation of colocalized pixels in each component of a dual-color image by calculating Pearson's correlation coefficient (PCC) and Manders' colocalization coefficients M1 and M2 with Costes' threshold.[51]

Calcium imaging video analysis

Acquired video files were analyzed in ImageJ (NIH). Regions of interest (ROIs) were assigned to 20-25 cells per video. Mean intensity values for each video frame were obtained and background fluorescence values were subtracted (giving the value ΔF). Subtracted data was normalized to $\Delta F/F_0 = (Fi-F_0)/F_0$, where Fi represents the intensity at the given time point and F_0 represents the average fluorescence of the first 10 frames. This data was low-pass filtered to reduce noise and averaged over 5 frames in Matlab (MathWorks, Natick, Massachusetts, USA). Traces were manually checked based on the timing of response and the shape of the transient to avoid including spontaneous rises in fluorescence. Maxima in the time window 45-65 s were used for a quantification and statistical comparison of different conditions.

Behavioral video analysis

Videos were cropped to the size of the arena, inverted in VirtualDub software and analyzed in the ToxTrac program with default settings,[44,52] which recorded the coordinates of the center of mass of each animal in each image frame during recording. Later all positional data were calibrated to the size of the arena as described[52] to obtain movement trajectories.

To quantitate the speed of propulsion along a trajectory, we measured the distance between animal position in every 50th video frame and divided by the corresponding time interval (0.125 s). We first assigned the status at each data point as either self-generated motion or quiescence, the latter defined as any speed lower than 0.09 mm/s, which was the speed observed for drift within the arena in the absence of tail movements. We distinguished two speed classes of self-generated motion related to the two specific movement types exhibited in the arena: swimming and idling. Swimming always involved forward propulsion of at least 1 animal length/s, which was always greater than 0.7 mm/s, whereas forward movement during idling was always less than 0.7 mm/s. Thus, drawing a line at 0.7 mm/s through a plot of speed versus time (as done in Figure 3) defined all points above the line as swimming intervals, and those below the line as idling intervals. To calculate the mean overall speed during a recording, speed data was filtered to eliminate speeds below 0.09 mm/s. Signal analysis of speed was based on identification of peak speeds during activity above the quiescence baseline. Peaks were identified automatically based on the speed threshold defined above. Activity and quiescence episode durations were calculated from waveform derivatives identifying the last inflection preceding and the first inflection following the peak.

Trajectory angle was defined as the complementary angle defined by three consecutive points in the trajectory. To characterize the types of activity (swimming and idling) of *O. dioica* in detail we calculated the trajectory angle for each consecutive set of 3 points of the trajectory and performed power spectral density analysis of the rate of change of trajectory angle (instantaneous frequency) to reveal the maximum instantaneous frequency during activity episodes for 10 randomly selected animals in the control condition. We evaluated the relation between the instantaneous frequency of trajectory angle and speed during swimming by simple linear regression analysis. All trajectory analysis was performed in Matlab (MathWorks, Natick, Massachusetts, USA) using built-in functions.

Statistics

Data are presented as standard box plots with mean, median, lower and upper quartiles, maxima, minima and outliers represented. Normality of data was tested by the Shapiro-Wilk normality test, and significance of differences between groups was determined by the Kruskal-Wallis test followed by post hoc Dunn's test with a Bonferroni correction or ANOVA followed by Tukey's post-hoc test or Mann-Whitney test and indicated as p-values (*p<0.05; **p<0.01; ***p<0.001). Data were analyzed and plotted in Excel (Microsoft, USA), in OriginPro 2020 (OriginLab Corporation, Northampton, USA) or in Matlab (MathWorks, Natick, Massachusetts, USA).